ECS Transactions, 68 (1) 2851-2858 (2015)
10.1149/06801.2851ecst ©The Electrochemical Society

Direct Ethanol Anode-Supported Solid Oxide Fuel Cell

S. D. Nobrega[a,c], M. C. Steil[a], S. Georges[a], S. Uhlenbruck[b], and F. C. Fonseca[c]

[a] Laboratoire d'Electrochimie et de Physicochimie des Matériaux et des Interfaces, UMR 5279, CNRS-Université de Grenoble, 38400 Saint Martin d'Hères, France
[b] Forschungszentrum Jülich GmbH, Institut für Energie- und Klimaforschung, 52428 Jülich, Germany
[c] Instituto de Pesquisas Energéticas e Nucleares, IPEN, 05508-000 São Paulo, SP, Brazil

An anode-supported solid oxide fuel cell (SOFC) was continuously operated with direct (anhydrous) ethanol for ~600 hours, with a high current density. The operation of the SOFC under ethanol was made possible with the deposition of a ceria-based catalytic layer onto the cermet anode support, which efficiently converts the primary fuel in hydrogen. The catalytic layer associated with the gradual internal reforming (GIR) process avoids carbon deposition on the Ni surface. The results provide a significant advance towards the development of direct ethanol solid oxide fuel cells.

Introduction

Solid oxide fuel cells (SOFCs) are promising devices for high efficient, environmentally friendly, and fuel flexible energy conversion (1,2). One of the main advantages of SOFCs, as compared to other fuel cells, is that the high operating temperatures (≥600°C) (1,2) allows to convert primary fuels (e.g., natural gas and ethanol) into hydrogen. The conventional Ni-based cermet anode exhibits excellent catalytic activity (3-9); however, the stable operation of SOFCs running on the fuels containing carbon is still a challenge because Ni promotes the dehydrogenation of fuel. Such reactions result in carbon deposition on the surface of the anode, causing a marked reduction in performance of the fuel cell (3-9). To avoid the deactivation of the conventional anode, the use of excess steam in the fuel has been used to prevent the thermodynamic conditions in which carbon deposition is favored (10). Such process is referred to as direct internal reforming. Nonetheless, the addition of large amounts of water in the fuel reduces the overall efficiency of the fuel cell system (10). Thus, carbon deposition on Ni-based composites has attracted attention to the modification of the SOFC anode material aiming at the operation using different fuels.

Among all the commercially available feedstocks for SOFC, including fossil fuels-derived such as hydrogen and natural gas, bioethanol has drawn increasing attentions as a promising SOFC fuel (8,11,12). Bioethanol is efficiently produced from renewable biomass, such as sugar cane, and is an economically viable energy source, producing low emissions and bringing positive impact to the economy and the environment (8,11,12). In addition, ethanol is a readily available liquid fuel allowing easy storage and transport.

To avoid the limitations caused by carbon formation in Ni cermets, alternative materials and anode designs are necessary to allow the stable operation of SOFCs with

carbon containing fuels. In this context, preserving the Ni cermet as the anode and adding a catalytic layer to allow the gradual internal reforming (GIR) has been pointed out as promising strategy (13-16). In the GIR process, the water released by the electrochemical oxidation of hydrogen at the anode is used for the steam reforming of the fuel in the catalytic layer deposited onto the anode (13,18,19). Ceria-based catalytic layers have been preferred due to the both the catalytic properties and the compatibility with the standard SOFC components (17,20). Thus, as long as the fuel cell is polarized, producing water, both the catalytic layer and electrochemical reactions sustain each other and the primary fuel is gradually consumed. Such a process has been demonstrated for ethanol and methane; however, previously reported results mainly concern electrolyte-supported SOFCs with relatively low current output (9,13,18-20,22). In the present study, a high-performance anode-supported SOFC was shown to run on (dry) ethanol in gradual internal reforming conditions without carbon deposition and excellent stability.

Experimental

The anode-supported single cells used in this study, with 8.03 cm^2 active area, were fabricated at Forschungszentrum Jülich[17]. The anode-supported cells present four layers: (i) electrolyte, 8 mol% yttria-stabilized zirconia – YSZ (32 mm diameter and ~10 µm thickness); (ii) cathode functional layer, strontium-doped lanthanum manganite - $La_{0.65}Sr_{0.30}MnO_3$ (LSM)-YSZ (50/50 wt%); (iii) cathode current collector, LSM (32 mm diameter and ~50 µm thickness); and (iv) anode substrate Ni-YSZ (42 mm diameter and ~600 µm thickness).

A catalytic layer of gadolinia-doped ceria ($Ce_{0,9}Gd_{0,1}O_{2-x}$, CGO), containing 0.1 wt.% of Ir (Ir-CGO), was added onto the anode support. The Ir-CGO catalyst was prepared by impregnation.[18] The appropriate amount of iridium acetylacetonate (Alfa Aesar) solution in toluene was added to a suspension of CGO. After evaporation of the solvent under reduced pressure, the catalyst was calcined in flowing O_2 at 350°C for 6 h. The Ir-CGO catalytic layer was deposited onto the anode by spray-coating technique using an ethanol/terpineol-based suspension with organic additives. After the coating step the catalytic layer was heated at 900°C for 2 h under argon flow (6 L h^{-1}). The total amount of the catalyst deposited in a single cell was 3 g, corresponding to a final thickness of the catalytic layer of ~120 µm (42 mm diameter).

Before catalytic layer deposition, a gold wire (0.5 mm thickness) was attached to the anode with gold ink, as the current collector. A platinum-mesh was attached to the cathode.

The anode-supported cell was fixed into an alumina support ring using a sealing glass paste. The support ring was fixed between two alumina concentric tubes, corresponding to the anode and cathode chambers. Alumina capillaries were inserted in the concentric tubes for both gas delivery and electric terminals. Four gold wires allow independent measurements of the current and the potential. The system was closed with metallic heads sealed with rubber gaskets. Fuel cell tests were performed at 850°C with flowing air (20% oxygen - 80% nitrogen) in the cathode side (10 L h^{-1}). Fuel cells were initially operated on H_2 (60%) and after anode reduction and stable OCV = 1.08 V, the electrochemical properties were studied under hydrogen and ethanol, without water

addition. Hydrogen (60%) was switched to the desired fuel ethanol (10%) using nitrogen as carrier gas. The fuel concentration was set to keep the theoretical number of electrons constant, and the liquid ethanol was kept in a thermal bath with a controlled temperature of 29°C and carried by nitrogen at total flow rate of 8 L h^{-1}. All the gas lines at the inlet of the anode were heated at ~90°C to avoid steam condensation. A simplified scheme of the experimental setup is given in Figure 1.

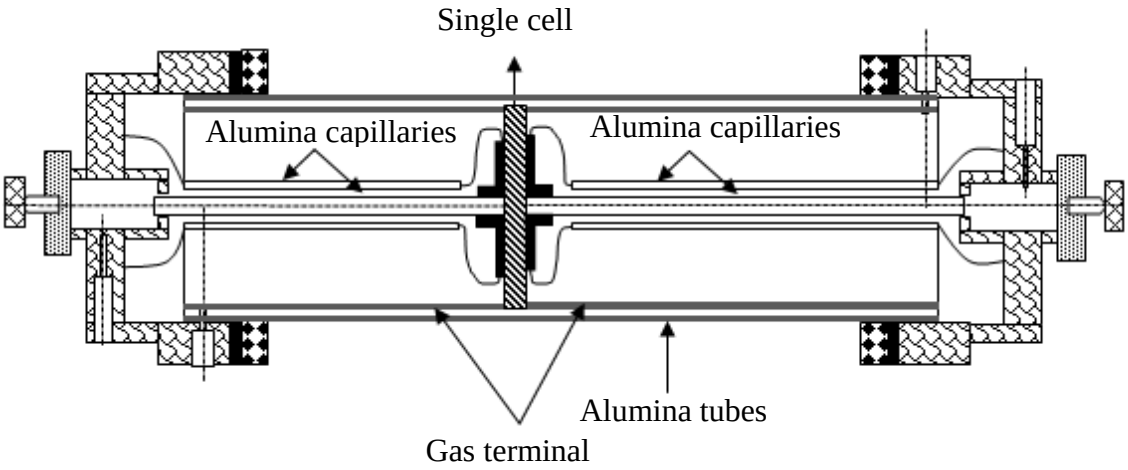

Figure 1. Scheme of the experimental setup for testing anode-supported fuel cells.

Electrochemical impedance spectroscopy (EIS) and polarization vs. time (i-*t*) measurements were performed by an Autolab PGSTAT128N potentiostat with a BSTR10A current booster. A variable resistor bench connected in series with the fuel cell was used for polarizations curve (V-i) measurements. Scanning electron microscopy and energy-dispersive X-ray spectra of the fractured surface of the anode were carried out after the fuel cell operation for ~650 hours.

Results and Discussion

The electrochemical properties of the fuel cell with the ceria-based catalytic layer were studied during operation on H_2/N_2 (60/40%) and C_2H_5OH/N_2 (10/90%). Before the ethanol tests, the optimization of the operation conditions was carried out in hydrogen. Initially, the total gas flows were adjusted, and the best ratio of fuel consumption and performance of the single cell was determined.

An optimization of the flows and ethanol concentration was defined as the fuel utilization (U_f) at the anode, which is dependent on the operating potential of the cell with the current obtained by the Faraday efficiency (ε_F). The Faraday efficiency is calculated by the ratio of the total current density (i_t) of the system and the potential current density obtained by the total consumption of hydrogen, determined from the flow rates, as shown in equation (1):

$$\mathcal{E}_{F} = i_t / i_i \qquad \text{(Eq. 1)}$$

The operation of the fuel cell was started with H_2/N_2 ratio of 10/90% with a total flow rate of 4 L.h^{-1} at the OVC. Gradually (in 2 hours), the relative amount of H_2 in the mixture H_2/N_2 ratio was increased stepwise (10%) until the 60/40% ratio was achieved.

Figure 2 shows the EIS diagrams taken at OCV (Fig. 2a) and the corresponding polarization curves (Fig. 2b) obtained at 850°C for the total flow rates of 4 L h^{-1}, 8 L h^{-1} and 12 L h^{-1}.

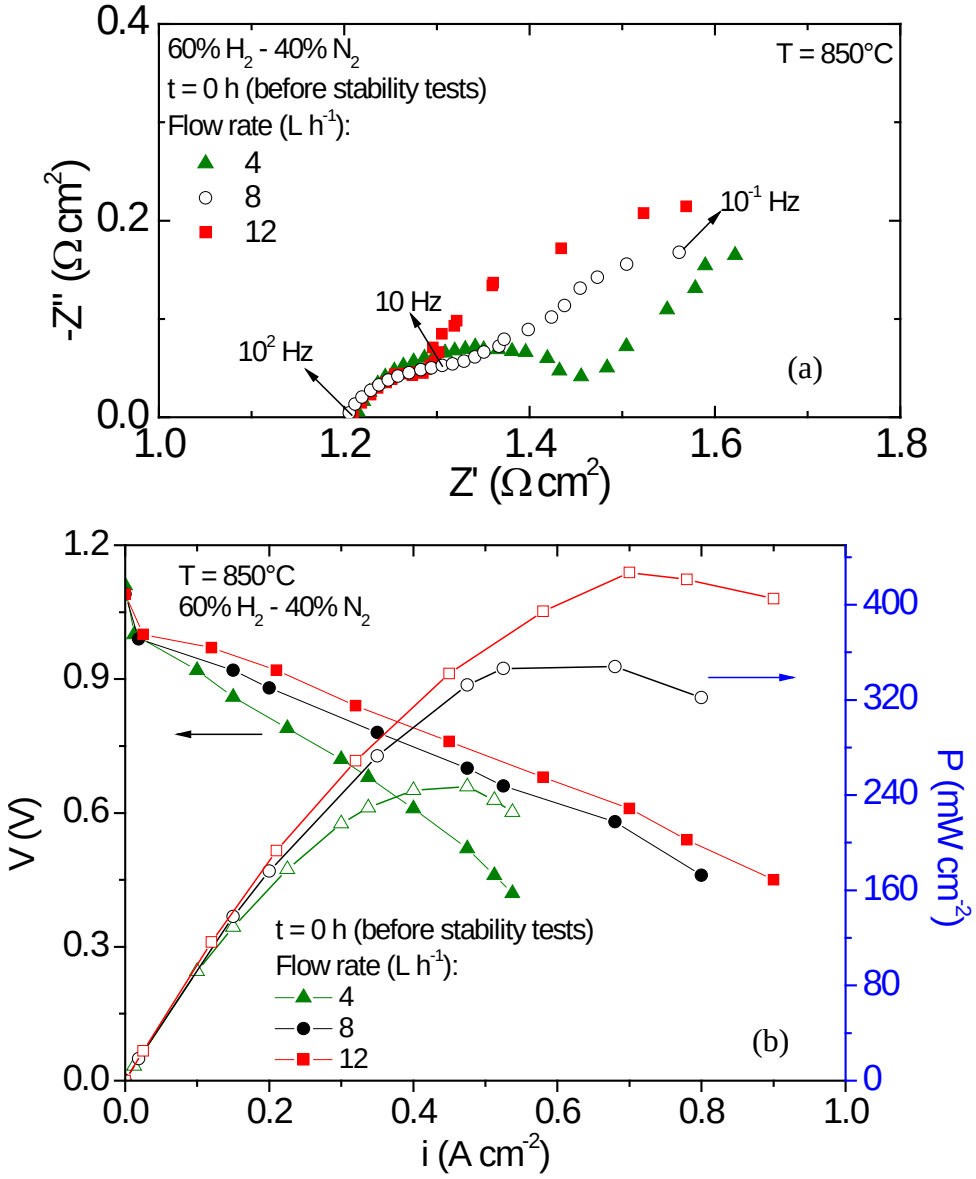

Figure 2. Impedance diagrams at OCV (a) and polarization curves (b) of a single cell operating with different flow rates running of hydrogen before the stability test.

The EIS diagrams exhibited convoluted contributions with a polarization resistance of ~0.25 Ω.cm² (4 L h^{-1}), 0.18 Ω cm² (8 L h^{-1}) and 0.1 Ω cm² (12 L h^{-1}), with a low frequency tail attributed to an additional diffusion resistance due to the porous catalytic layer (19). The polarization curves were recorded from the OCV (1.08 V) to 0.4 V at different fuel flow rates at 850°C (Fig. 2b). At 0.6 V, power densities were ~235 mW.cm^{-2} (4 L.h^{-1}), 350 mW.cm^{-2} (8 L.h^{-1}) and 410 mW.cm^{-2} (12 L.h^{-1}).

Assuming a ε_F = 1 for the electrochemical oxidation of H_2, the fuel utilization (U_f) was adjusted for the stability tests (9,19). According to the model describing both the catalytic and the electrochemical reactions, a minimum U_f must be achieved to ensure enough steam release from the anode for the complete conversion of the fuel in the

catalyst layer. If the fuel cell produces insufficient steam to ensure the complete conversion of the fuel it is likely that fuel diffusion into the Ni-YSZ cermet and carbon deposition occur. Figure 3 shows the dependence of the U_f with the flow rate, at 0.4 V, 0.6 V, and 0.8 V. The U_f decreases with increasing fuel flow rate. In the case of ethanol, respecting the 1/6 ratio to hydrogen, prevented the increase of the fuel concentration. Thus, U_f was set at ~37%, corresponding to the flow rate 8 L h^{-1} (0.6 V).

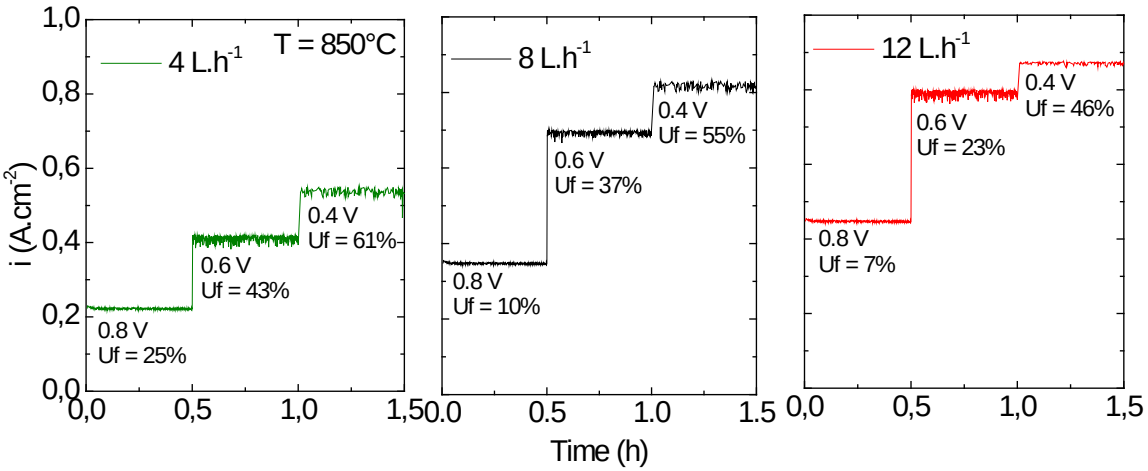

Figure 3. Fuel utilization for hydrogen under polarization at 0.8 V, 0.6 V, and 0.4 V, for different total flow rates.

Figure 4 shows the time dependence of i at 0.6 V using H_2 and ethanol. The operation of the fuel cell was started with H_2/N_2 (60/40 %) with a flow rate of 8 L.h^{-1} at 0.6 V. After 5 hours of operation, the anode atmosphere was gradually changed to 10% of ethanol. This change was made ensuring a constant supply of fuel to keep the current density at fixed polarization (0.6 V) of the cell. While dry ethanol is fed into the catalytic layer, the cell must remain polarized to ensure the formation of steam necessary for the catalytic conversion.

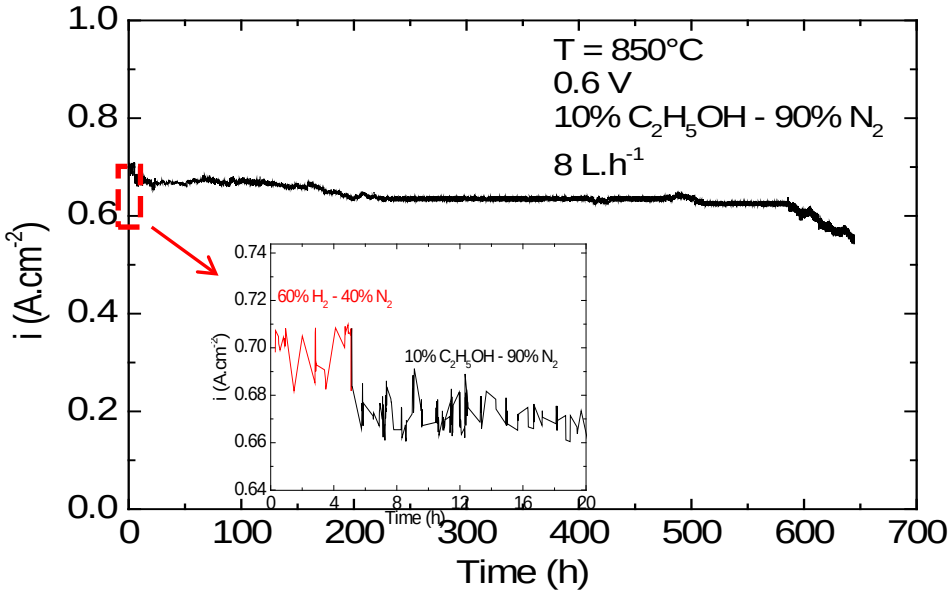

Figure 4. Potentiostatic test at 0.6 V of the single SOFC containing a ceria-based catalytic layer under anhydrous ethanol. The inset shows the expanded initial hours of the test when hydrogen was changed to ethanol.

The inset of Figure 4 shows the transition from hydrogen to ethanol. After 5 h on H_2, the fuel was changed to ethanol / nitrogen (10/90%) and a slight reduction of i, from ~0.70 Acm^{-2} (H_2) to 0.67 Acm^{-2} (ethanol), was observed. Nevertheless, the most important result of Figure 4 is the stable operation of the fuel cell for ~650 h using dry ethanol. The operation of the cell for 650 h with excellent stability is a strong indication that ethanol has been converted in the catalytic layer without carbon deposition on the anode. It is important to consider that ethanol chemistry at the SOFC operating temperature is complex and a considerable fraction of the alcohol is pyrolysed before reaching the catalytic layer. Nonetheless, the Ir-CGO layer is designed to efficiently convert main ethanol pyrolysis products, such as CH_4 (9,22,23). The catalytic tests confirmed that no undesirable by-products, such as acetaldehyde and ethylene, resulting from the reactions of dehydrogenation and dehydration of ethanol were formed. Acetaldehyde and ethylene inhibit the production of H_2 and promote carbon formation, preventing the stable operation of the fuel cell (9). Therefore, the experimental results shown in Fig. 4 confirmed that Ir-CGO catalyst was active and efficient for fuel cell operation with dry ethanol by the gradual internal reforming. During the last ~50 hours of testing the current output decreased possibly due to sealing related problems that are currently under investigation.

To investigate possible degradation due to carbon deposition on the surface of the anode, scanning electron microscopy and energy dispersive spectroscopy analyses were performed after the operation of the fuel cell, as shown in Figures 5 and 6. After ~ 650 h of operation with anhydrous ethanol, the anode microstructure showed no apparent deposition of carbon (Fig. 5). This observation was confirmed by energy dispersive analysis (Fig. 6). The small sign related to carbon is associated with possible formation of non-graphitic deposits, which can be easily oxidized and represent no major harm to fuel cell performance (9).

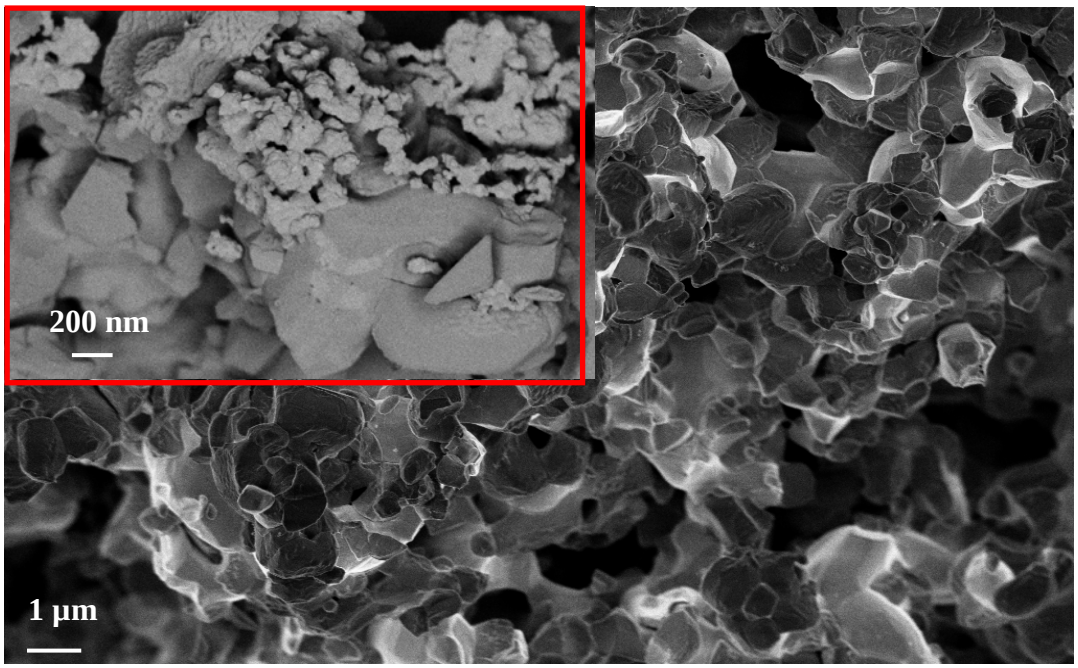

Figure 5. Scanning electron micrograph of the anode after 650 hours of operation under anhydrous ethanol.

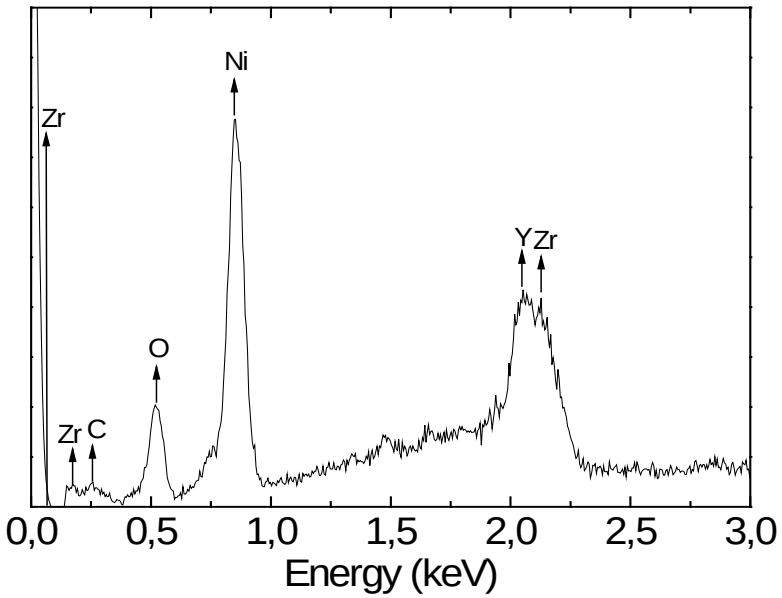

Figure 6. Energy dispersive X-ray spectroscopy of the anode after 650 hours of operation under anhydrous ethanol.

Conclusions

A high performance anode-supported SOFC was designed for direct dry ethanol operation without carbon deposition. A standard anode-supported single cell, associated with a catalytic layer of Ir-CGO deposited onto the Ni-YSZ anode, was operated under gradual internal reforming conditions with good stability without adding steam, or any oxidizing agent, for ~650 hours. The experimental results demonstrate the efficiency of ethanol conversion in solid oxide fuel cells. Such results are strong evidence that high-current output fuel cells can operate in gradual internal reforming using carbon containing fuels provided that an active catalyst is available.

References

1. S.C. Singhal and K. Kendall, *High Temperature and Solid Oxide Fuel Cells – Fundamentals, Design and Applications*, p. 1 (2003).
2. N.Q. Minh, *J. Am. Ceram. Soc.*, **76**, 563(1993).
3. A. Atkinson, S. Barnett, R.J. Gorte, J.T.S. Irvine, A.J. McEvoy, M. Mogensen, S.C. Singhal and J. Vohs, *Nat. Mater.*, **3**, 17 (2004).
4. J. Liu and S.A. Barnett, *Solid State Ionics*, **158**, 11 (2003).
5. Z. Zhan and S.A. Barnett, *J. Power Sources*, **155**, 353 (2006).
6. M. Liao, W. Wang, R. Ran and Z. Shao, *J. Power Sources*, **196**, 6177 (2011).
7. B. Huang, X. Zhu, W. Hu, Y. Wang and Q. Yu, *J. Power Sources*, **195**, 3053 (2010).
8. G.A. Deluga, J.R. Salge and X.E. Verykios, *Science*, **303**, 993 (2004).
9. S.D. Nobrega, P. Gelin, S. Georges, M.C. Steil, B.L. Augusto, F.B. Noronha and F.C. Fonseca, *J. Electrochem. Soc.*, **161**, F354 (2014).
10. R.J. Gorte and J.M. Vohs, *J. Catal.*, **216**, 477 (2003).

11. M. Ni, D.Y.C. Leung and M.K.H. Leung, *Int. J. Hydrogen Energ.*, **32**, 3238 (2007).
12. E.N. Armstrong, J. Park and N.Q. Minh, *Electrochem. Solid-State Lett.*, **15**, B75 (2012).
13. P. Vernoux, J. Guindet and M. Kleitz, *J. Electrochem. Soc.*, **145**, 3487 (1998).
14. J. Liu and S.A. Barnett, *Solid State Ionics***, 158**, 11 (2003).
15. M. Liao, W. Wang, R. Ran and Z. Shao, *J. Power Sources***, 196**, 6177 (2011).
16. S. P. Jiang, Y. Ye, T. He and S.B. Ho, *J. Power Sources***, 158**, 179 (2008).
17. F.C. Fonseca, S. Uhlenbruck, R. Nédélec and H.P. Buchkremer, *J. Power Sources*, **195**, 1599 (2010).
18. J.M. Klein, M. Hénault, C. Roux, Y. Bultel and S. Georges, *J. Power Sources*, **193**, 331 (2009).
19. J.M. Klein, M. Hénault, P. Gélin, Y. Bultel and S. Georges, *Electrochem. Solid-State Lett.*, **11**, B144 (2008).
20. B.L. Augusto, F.B. Noronha, F.C. Fonseca, F.N. Tabuti, R.C. Colman and L.V. Matos, *Int. J. Hydrogen Energ.*, **39**, 11196 (2014).
21. M.Li, B. Hua, J. Pu, B. Chi and J. Li, *Int. J. Hydrogen Energ.*, 39, 15975 (2014).
22. J.M. Klein, S. Georges and Y. Bultel, *J. Electrochem. Soc.*, **155**, B333 (2008).
23. M. Wisniewski, A. Boréave and P. Gélin, *Catal. Commun.*, **6**, 596 (2005).
24. S.D. Nobrega, M.V. Galesco, K. Girona, D.Z. de Florio, M.C. Steil, S. Georges and F.C. Fonseca, *J. Power Sources*, **213**, 156 (2012).